PERGAMON

Microelectronics Reliability 41 (2001) 571–578

MICROELECTRONICS RELIABILITY

www.elsevier.com/locate/microrel

Thermal modeling of single event burnout failure in semiconductor power devices

D.G. Walker [a,*], T.S. Fisher [a], J. Liu [b], R.D. Schrimpf [b]

[a] Department of Mechanical Engineering, Vanderbilt University, Box 1592, Station B, Nashville, TN 37235, USA
[b] Department of Electrical Engineering, Vanderbilt University, Box 1824, Station B, Nashville, TN 37235, USA

Received 23 May 2000; received in revised form 3 October 2000

Abstract

Experimental investigations of single event burnout (SEB) of power devices due to heavy ion impacts have identified the conditions required to produce device failure. A key feature observed in the data is an anomalistic secondary rise in current occurring shortly after the ion strike. To verify these findings including the thermally induced secondary plateau, simulations have been performed on the model single event burnout. The new models include additional thermally dependent electrical components to capture thermally induced physical effects. Through the inclusion of analytic temperature models coupled with the electrical model, the electrical response is predicted with reasonable accuracy. The simulations provide order-of-magnitude estimates as well as prediction of phenomenological features such as the secondary rise in current. This work represents a first attempt to characterize thermal failure of power devices due to heavy ion impacts by including temperature dependent components that until now have not been modeled. The thermal model in the present work produces qualitative agreement with experiments on SEB that have been previously unexplained.

1. Introduction

Single event burnout (SEB) failure of power devices may result from heavy ion impacts that occur in space environments [1,2]. The failure of electronic components in satellites and high-altitude aircraft that operate in ion rich environments can result in mission failure. Research on SEB in power devices can reduce the occurrence of catastrophic failures of power devices and thereby increase the survivability of aerospace systems. The ability to model SEB events can augment the design process, leading to more reliable devices and equipment that depend on these devices. Because the breakdown mechanism is thermal in nature, the investigation of the transport of thermal energy is crucial to successful modeling. This work represents a first attempt to characterize thermal failure of power devices due to heavy ion impacts.

SEB is triggered when a heavy ion passes through a power MOSFET biased in the "off" state (blocking a high drain–source voltage). As a high energy ion travels through the device, a path of electron–hole pairs is created [3]. As a result, a current filament along the path of the ion develops. This initial, short-lived current may cause the MOSFET to "turn on". Once the MOSFET has been activated in this way, the device may remain on due to a parasitic bipolar-junction transistor (BJT) inherent in the device [4].

The source, body, and drain regions of the MOSFET comprise the emitter, base, and collector regions of the parasitic BJT. The BJT is the mechanism by which the MOSFET is activated by the ion strike. During normal operation of the power MOSFET, this parasitic BJT is always turned off due to the common source-body metallization that shorts the base–emitter junction. Once the BJT is turned on by an ion strike, collector currents in the BJT increase to the point where second breakdown can occur, creating a permanent short between the

* Corresponding author. Tel.: +1-615-343-6959; fax +1-615-343-6687.
E-mail address: greg.walker@vanderbilt.edu (D.G. Walker).

0026-2714/01/$ - see front matter
PII: S0026-2714(00)00249-3

Nomenclature

α	thermal diffusivity	η	thermal penetration depth (cm)
E_g	band gap energy (Joule)	P	power dissipated (W)
g	volumetric generation rate (W/m^3)	q	electron/hole charge (coulomb)
k	thermal conductivity (W/m^2 K)	r	radius (μm)
k_B	Boltzmann constant (1.38×10^{-23} J/K)	T	temperature (K)
N	effective density of states (cm^{-3})	t	time (μs)
n_i	intrinsic carrier concentration (cm^{-3})	μ	carrier mobility (cm^2/Vs)

source and drain. This secondary breakdown is a direct result of a thermally-induced regenerative feedback mechanism [5].

Numerous studies have investigated the SEB mechanism and its effects on power MOSFETs [6]. Models developed to explain the SEB phenomenon have been very helpful in gaining insight into the physical failure mechanisms that contribute to SEB. An SEB circuit model has been developed for understanding the effects of various circuit parameters [7]. However, one particular artifact observed in experimental data has eluded mathematical description. A secondary rise in current has been recorded by Johnson et al. [5] and by Roubaud et al. [8] which starts after the device has reached an apparent steady operating condition. The current then rises over a short period of time to reach another plateau. The phenomenon is reported to be the result of a thermal mechanism, but no supporting evidence is provided.

Modeling and simulation of SEB remain as important methods of determining why heavy ion impact results in destructive currents and provide a means for performing virtual experiments that are less expensive than physical tests. However, thermal energy dissipation has often been ignored in analyses. It is accepted that the failure mechanism is ultimately a result of thermal melt-down, but the effect of the energy generation on the electrical properties and behavior has not been previously considered in detail.

Approximations of the amount of Joule heating from voltage and current measurements as a result of self-maintaining currents from heavy ion collisions range from 5 W [8] to nearly 100 W [9]. Furthermore, the generation of this power is concentrated in a small region [6] and lasts for several microseconds (until the device is turned off to prevent melt-down). These values are indicative of nonuniform effects as described by Apanovich et al. [10] whose work on electrothermal simulation of semiconductor devices indicates that simulation must incorporate nonisothermal effects to eliminate inaccuracies for devices with large temperature gradients. Methods for coupling the thermal distribution and the electrical performance through compact models have been described in Ref. [11] for IBGTs. However, this approach gives a global distribution which is not necessarily applicable for a single device. The present work represents a characterization of the influence of temperature on relevant transport mechanisms and device performance.

The objective of this work is to characterize the generation of thermal energy in SEB of power devices using an analytic thermal conduction solution coupled with a circuit-level electrical simulation. From the temperature fields obtained in this analysis, electrical parameters such as carrier concentration and mobility, which are highly coupled to the thermal response, are inferred. Also, the thermal simulations are coupled to SPICE circuit simulations to demonstrate the effects of increased temperature on device performance. Lastly, the assumptions concerning the generation region are investigated through parametric studies of temperature as a function of the geometry of the region of heat generation.

2. Theory and model development

2.1. Electrical model

The SEB process can be modeled as an electrical circuit shown in Fig. 1 [7]. Several key elements are used to model the SEB process. A steep linear ramp in current

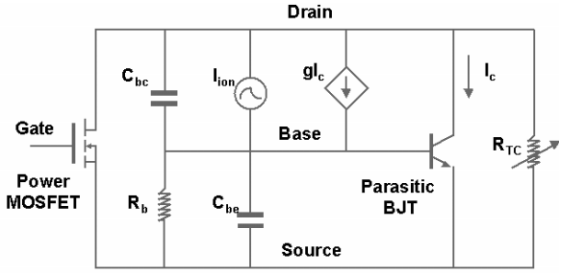

Fig. 1. Electrical circuit used to model SEB of power MOSFETs.

represents the initial current pulse at the junction. A resistor connects the body region to the source, which corresponds to the base resistance in the SEB analytical model [6]. When a heavy ion hits the device, the deposited charges will charge the RC circuit and raise the base voltage. Depending on how high the initial base voltage is increased, the parasitic BJT may be turned on. A feedback mechanism is then established which is modeled by a current-controlled current source in the circuit model. The thermal effect on the device is represented by a variable shunt resistance R_{TC} in parallel with the parasitic BJT.

The only components in the SPICE model implemented here that are temperature dependent are the parasitic BJT and the shunt resistance. The temperature dependence of the transistor is controlled by SPICE's model parameters. The current and voltage are exponential functions of temperature, but they vary in opposite directions. Therefore, the power dissipated is a weak function of temperature. As a result, the model without the shunt resistance produces negligible effects as the temperature is changed. The shunt resistance, then, is the single most important component when incorporating temperature effects, and is primarily responsible for the results reported here. The evaluation of this resistance is described in a subsequent section.

2.2. Analytic conduction model

The transient, nonhomogeneous diffusion equation is solved analytically for boundary conditions and properties representative of an operating power device undergoing a heavy ion strike (see Fig. 2 for computational domain). To find a solution, we assume that the heat generation occurs in a cylindrical region surrounding the current filament, and the governing equation is solved in an axisymmetric cylindrical coordinate system.

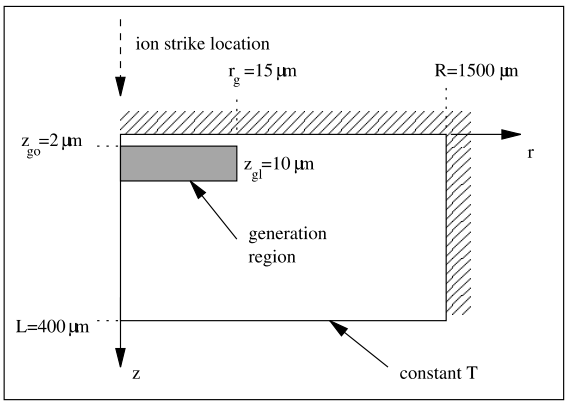

Fig. 2. The computational domain is cylindrical where the current filament lies along the center line.

$$\frac{1}{r}\frac{\partial}{\partial r}\left(r\frac{\partial T}{\partial r}\right)+\frac{\partial^2 T}{\partial z^2}+\frac{g}{k}=\frac{1}{\alpha}\frac{\partial T}{\partial t} \tag{1}$$

$$T(t=0)=0 \quad \text{initial condition} \tag{2}$$

$$\left.\frac{\partial T}{\partial r}\right|_{r=0}=0 \quad \text{symmetry}, \qquad \left.\frac{\partial T}{\partial r}\right|_{r=1}=0 \quad \text{insulated} \tag{3}$$

$$\left.\frac{\partial T}{\partial z}\right|_{z=0}=0 \quad \text{insulated}, \qquad T(z=L)=0 \quad \text{semiinfinite} \tag{4}$$

In Eq. (1), g is a constant heat generation rate per unit volume, and the thermal conductivity, k, and thermal diffusivity, α, are assumed to be independent of temperature. The boundary conditions for the disk-shaped semiinfinite conduction domain (depicted in Fig. 3) are symmetry at the centerline and insulated in the far-field (Eq. (3)). The top of the device is insulated and the bottom is held at a constant temperature (Eq. (4)). The double infinite sum solution follows from Ref. [12].

$$T(r,z,t)=\frac{4g\alpha}{R^2Lk}\sum_{m=0}^{\infty}\sum_{n=0}^{\infty}[1-\exp(-At)] \times \frac{J_0(\beta_m r)}{J_0(\{\beta_m R)}\cos(v_n z)G/A \tag{5}$$

$$\beta_m \leftarrow \text{ positive roots of } J_1(\beta R)=0$$
$$v_n \leftarrow \text{ positive roots of } \cos(vL)=0$$
$$A=\alpha(\beta_m^2+v_n^2)$$
$$G=\int_0^{r_g}\frac{J_0(\beta_m R')}{J_0(\beta_m R)}\mathrm{d}r'\int_{z_{g0}}^{z_{g0}+z_{gl}}\cos(v_n z')\mathrm{d}z'$$

The geometry of the conduction problem is correlated to the geometry of the device shown in Fig. 3. The centerline of the conduction region corresponds to the location of the ion strike where the charge carrier flow is greatest during the burnout event. Therefore, Joule

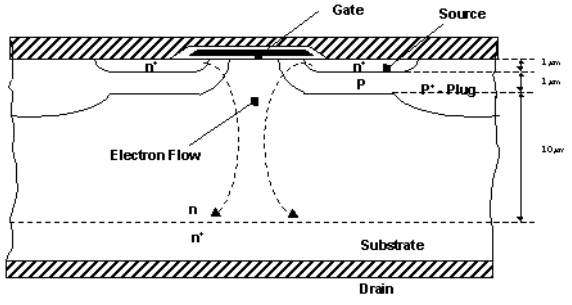

Fig. 3. The dimensions of a typical MOSFET device were used as guidelines for determining the computational domain of the conduction analysis.

heating occurs about the ion strike location in the n-region (epitaxial) which is the centerline of the conduction domain. Because of the time scales used in this analysis, it can be assumed that the conduction domain in the axial and radial directions are semiinfinite. In other words, the chip dimensions (400 μm in the z-direction from Fig. 3) are much larger than the generation region dimensions (10 μm). However, the generation region is thermally close to the top surface of the chip, therefore, the top boundary condition may influence the solution significantly.

The generation region is specified by a radius of influence, r_g, the longitudinal location, z_{go}, and a thickness, z_{gl}, as shown in Fig. 2. The values for the location and thickness were taken to be $z_{go} = 2$ μm and $z_{gl} = 10$ μm respectively. The radius of the generation region was a free parameter in the problem and could take a value from the radius of the current filament to the size of a single cell of the MOSFET. The power (P), dissipated in this region due to Joule heating, is estimated from circuit voltages and currents. The heat dissipated is related to the electrical power by the volume in which generation occurs ($g = P/V$); therefore, the effects of size and location can significantly influence the results.

The conduction solution predicts a temperature field from which a representative temperature must be chosen. This representative temperature is passed to the electrical analysis as the operating temperature of the circuit. Within the generation region, the temperature distribution is relatively flat, so the maximum temperature is used to model the temperature effects in the circuit analysis. This temperature was used to calculate an effective shunt resistance from temperature-dependent device physics (see Section 2.3).

The solution of Eq. (1) involves integral transforms and produces an infinite series [12]. The computation of the series was verified for convergence and accuracy by testing against other known one-dimensional solutions. Furthermore, the transient solution was seen to approach the independent two-dimensional steady-state solution. Additionally the number of terms used in the two-dimensional transient analysis was increased by an order of magnitude to ensure convergence (as we are not especially concerned with computational efficiency here).

2.3. Shunt resistance model

The shunt resistance included in the SPICE circuit represents the primary coupling between the thermal analysis and the electrical circuit model. Even though temperature dependence is built into the BJT in the circuit, its dependence is relatively weak compared to the effects of the shunt resistor once the temperature becomes sufficiently high.

Because the resistor represents the electrical resistance through the epitaxial layer of the power MOSFET, its magnitude is largely governed by the intrinsic carrier concentration, n_i, in the device (see Ref. [13]).

$$R_{TC} = \frac{1}{q\mu n_i}\frac{l}{A} \tag{6}$$

Here, q is the charge of the carriers, μ, the mobility of the carriers, l, the length of the epitaxial region or the distance through which the current flows, and A, the area of the resistor. Note that the mobility is treated as a constant in this case because its dependence on temperature is much weaker than that of n_i.

At normal operating temperatures, R_{TC} is very large and does not play a significant role in the circuit. As the temperature increases, the shunt resistance decreases until it eventually dominates the electrical conduction. The intrinsic carrier concentration and the area are both functions of temperature that cause the resistance to decrease with temperature.

The resistance area is a circular region defined by the radius of the generation region plus a distance defined by the penetration depth of the thermal energy. It is assumed that the penetration depth can be expressed in terms of the thermal diffusivity and time ($\eta = \sqrt{\alpha T}$). The energy generated from Joule heating diffuses into the surrounding area, raising the temperature outside the generation region and increasing the effective area of the shunt resistance. The increase in effective resistive area also affects the strength of the generation rate. Because the current is flowing through a larger area, the generation also occurs in a larger volume, thereby decreasing the power per unit volume dissipated.

The intrinsic carrier concentration is used in the modeling of the shunt resistor because at high temperatures its influence will become larger than that of the doping. The temperature-dependent carrier concentration [13] is given as

$$n_i = \sqrt{N_C N_V}\exp\left[-\frac{E_g}{2k_b T}\right] \tag{7}$$

where the effective density of states for the conduction band, N_C, and the valence band, N_V, are evaluated for silicon. The effective density of states for silicon can be written as [14]

$$N_C = 2.8\times 10^{19}\left(\frac{T}{300}\right)^{3/2}\text{cm}^{-3} \tag{8}$$

$$N_V = 1.04\times 10^{19}\left(\frac{T}{300}\right)^{3/2}\text{cm}^{-3} \tag{9}$$

Further, the band gap energy, E_g, is a function of temperature given empirically [13] for silicon as

$$E_g = 1.17 - 4.73 \times 10^{-4} \frac{T^2}{T + 636} \text{ eV} \quad (10)$$

Initially temperature is not a factor in controlling the shunt resistance. At normal operating temperatures, the dopant concentration overwhelms the intrinsic concentration. This initial concentration is accounted for in the model of the MOSFET in SPICE and is therefore not considered in the shunt resistance. Once the intrinsic concentration due to a rise in temperature exceeds the dopant concentration, the shunt resistance becomes significant in the over-all model.

3. Results

3.1. Conduction solution

The temperature of most interest is the maximum temperature, which strongly affects electrical behavior. The power dissipated was estimated from experimental data (without the secondary peak) and circuit level analysis to be approximately 8 W. Fig. 4 shows the maximum temperature for this power level. After 0.5 μs, the temperature is greater than 600 K, which approaches the melting temperature of aluminum. Even though the melting temperature of aluminum may not be a deciding factor in the survivability of a device, it demonstrates the potential for catastrophic failure. Clearly, temperature is a significant factor in the electric behavior of the device long before melt-down actually occurs.

Note that the location of the maximum temperature is initially at the vertical center of the generation region on the centerline. With increasing time, the boundary conditions (namely the insulated top surface of the chip) begin to influence the solution, and as a result, the location of maximum temperature moves towards the top of the device. Fig. 5 displays the distribution of temperature at the centerline of the device for different times.

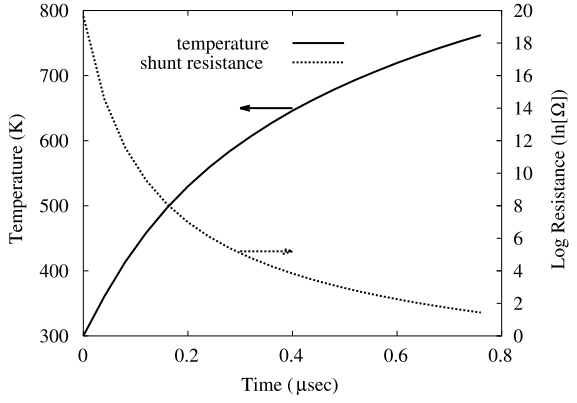

Fig. 4. The maximum temperature in a device dissipating 8 W. The shunt resistance as a function of temperature will not affect the device until 0.4 μs.

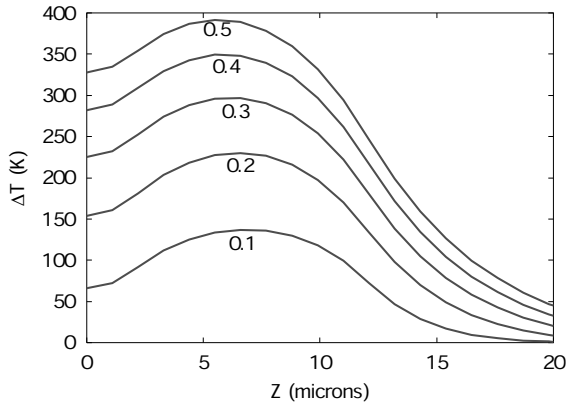

Fig. 5. The temperature distribution along the location of the current filament (center line) for different times in μs.

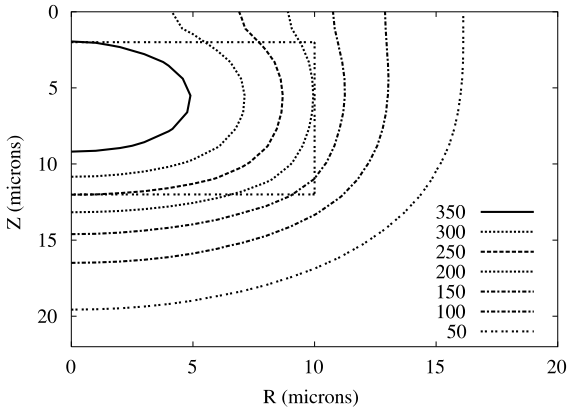

Fig. 6. Temperature contours at $t = 0.5$ μs indicate the localization of the heat generation. The box indicates the heat generation region.

The localization of temperature is illustrated in Fig. 6, which shows the temperature rise near the generation site at 0.5 μs. Even though the central temperatures are very high, the energy has not diffused far from the generation site, and large gradients occur. For this reason, the maximum temperature can provide a good estimate of the representative temperature of the circuit. At $t = 0.5$ μs, the maximum heat flux can be estimated using Fourier's law to be 10^9 W/m^2, which is roughly two orders of magnitude greater than the flux on the surface of the Sun.

3.2. Circuit-level results

Without including the temperature as a feedback parameter in the circuit analysis, we can obtain an estimate of the power dissipated in a power device as a

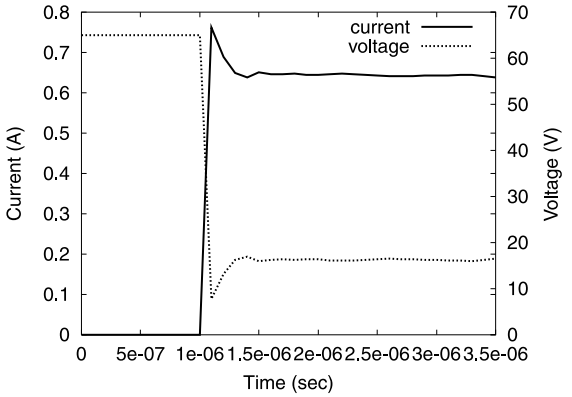

Fig. 7. Typical voltage and current response due to a heavy ion strike at $t = 1$ μs calculated from a circuit level analysis without thermal effects.

result of an ion strike. From Fig. 7, we notice that the device is "turned on" by the ion strike at $t = 1$ μs. The device then remains on because of the feedback in the equivalent circuit. If there were no thermal failure mechanisms, this would be a stable condition. For the circuit parameters selected [7] and without incorporating the temperature rise, there is no evidence of a secondary rise in the current. Note that without the shunt resistor, an increase in temperature does not significantly affect the results shown despite the fact that the BJT is temperature dependent.

Using the current and voltage time histories, the average power dissipated can be estimated to be approximately 8 W. Recall that the results in Fig. 4 indicate temperature rises greater than 300 K for 8 W of heat dissipating in a single cell of the power MOSFET device. Therefore, we can expect a similar temperature rise for this particular device.

3.3. Coupled electrical/thermal results

As stated earlier, the primary goal of this work is to introduce thermal analysis into the circuit level electrical analysis and to describe a phenomenon reported by Roubaud et al. [8] in MOSFETs and again by Lorfevre et al. [9] in IGBTs. Given appropriate conditions, power devices have been known to exhibit a secondary increase in current between 0.3 and 0.6 μs after the ion strike. Representative data from these studies are given in Fig. 8(a) and (b). It is believed that the secondary increase in current is caused by a large increase in temperature. We have seen that the Joule heating resulting from the ion strike can cause a device to reach temperatures near survivability limits of some device elements.

The coupling of the temperature solution and SPICE was accomplished by controlling each component and the time stepping independently. For each time step, a

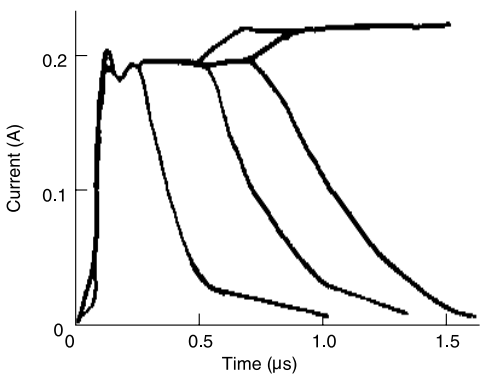

(a)

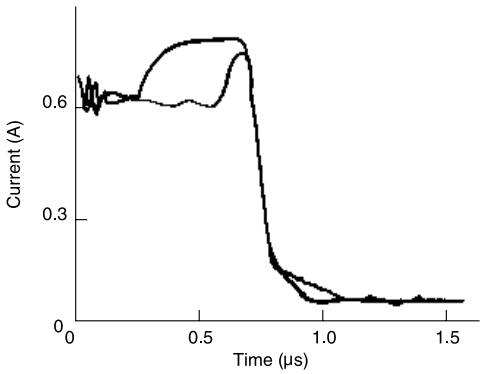

(b)

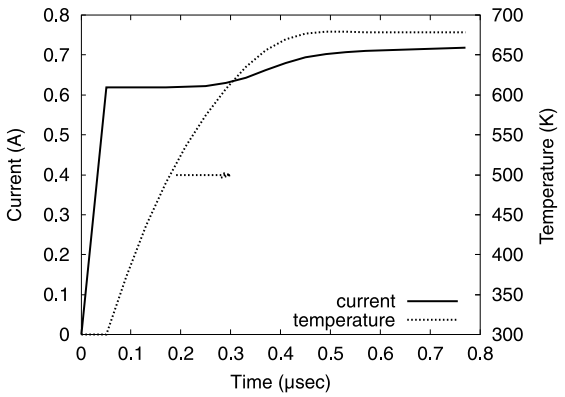

(c)

Fig. 8. Representative experimental data reported in (a) Ref. [5] and (b) Ref. [8] along with (c) simulated current response and temperature history. The start time corresponds to the primary ion strike.

temperature using the conduction solution and Duhamel's theorem for an arbitrarily varying generation rate was obtained. The resulting maximum temperature was then used as the component temperature in the SPICE model and in the shunt resistance calculation. Between each step the current "state" of the electrical analysis was recorded so it could be reset to start the analysis for the subsequent time step. This integration approach is similar to that used by Petegen et al. [15]. Note that with this scheme the temperature signature lags the electrical analysis by one time step. As the time step decreases, the coupled solution reaches a self-consistent state.

The primary result of the coupled analysis is the prediction of a secondary peak in the current that resembles the experimental data (see Fig. 8(c) compared to Fig. 8(b)). The agreement between the new physical model and the experiments validates the SPICE model as well as the temperature coupling in the shunt resistance. The temperature rise occurs at about the same time with a similar increase in magnitude as observed in experimentation. However, the rate at which the predicted rise occurs is somewhat less than that of the experimental data. The physical model further predicts that the voltage across the device drops (due to the shunt resistance), which causes the power dissipated to drop as well (Fig. 9). After the secondary peak, the device reaches a steady state where the Joule heating is balanced by the heat diffusion away from the device. Therefore, a constant temperature distribution is achieved. The physical model suggests that if the steady temperature is lower than destructive temperatures associated with the device, thermally-induced catastrophic failure will not occur. However, survival of a device under these conditions has not been observed experimentally.

Several analytical approximations affect the ability of the coupled model to match the experimental data more precisely. The more influential factors include the characteristic temperature used to represent the temperature of the entire device. The analytic conduction solution is capable of generating a temperature field, but we must select a single temperature for the circuit analysis. Similarly, the generation region shape and size will influence the results. In our case, we assumed a cylinder that extended over the epitaxial region using the radius as a free parameter. In reality the generation is not confined to and is not constant through the defined region. Despite these approximations along with other standard assumptions such as constant thermal properties, the present model predicts the occurrence of the secondary current rise. More detailed modeling should improve the model's ability to predict the event's onset time, rise time and magnitude.

As mentioned previously, devices that experience temperature increases in such short time periods are often thrown out of thermodynamic equilibrium. A device is considered to be out of equilibrium when the local energy carriers in the device have significantly different energy levels. This effect was not considered in this simplified model. Additional research that includes electrothermal modeling of statistical device physics is needed to resolve nonequilibrium effects.

3.4. Generation region

Using the data acquired in Section 3.3 as a baseline, the effect of the size and shape of the generation region on the secondary rise in current can be investigated. The free parameter in this case is the radius of the generation region. As the radius decreases, we expect the temperature to increase because the same amount of power is being dissipated in a smaller region. If we take the radius of the generation region to be of the order of the current filament, unreasonable temperatures are calculated.

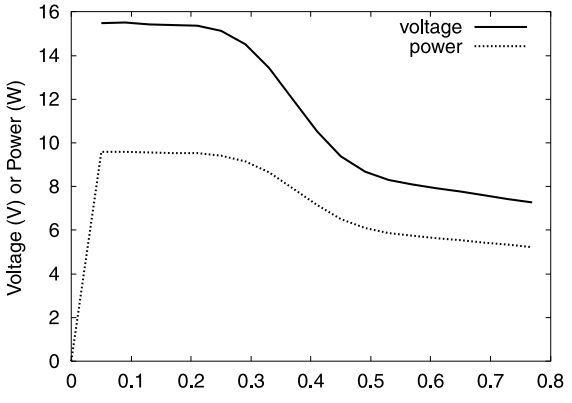

Fig. 9. The voltage across the device drops as the shunt resistance increases. The power also drops despite a corresponding rise in the current.

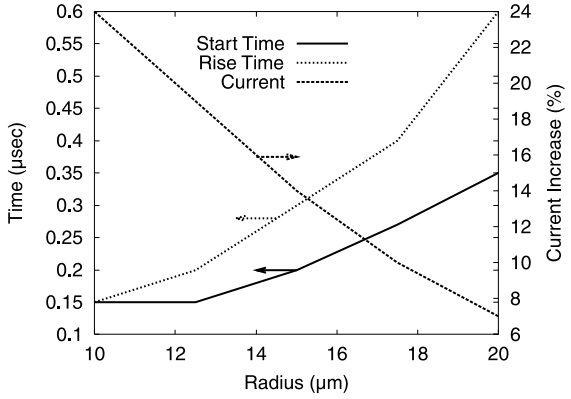

Fig. 10. Secondary peak metrics as a function of generation region radius.

Table 1
Secondary peak metrics for data displayed in Fig. 8[a]

Metric	Experimental (a)	Experimental (b)	Simulated (c)
Start time (μs)	0.5	0.3	0.2
	0.75	0.65	
Rise time (μs)	0.2	0.1	0.3
	0.2	0.15	
Current rise (%)	16	25	14
	16	24	

[a] Experiment (a) is from Ref. [5] and experiment (b) is from Ref. [8].

Therefore, the region must be larger than the radius of the filament. The range of values for the radius that produce reasonable results is shown in Fig. 10. The metrics that identify the character of the peak are the start time, the rise time and the increase in current. As expected, a larger radius smoothes the peak out and delays its onset because the temperature does not rise as rapidly. For comparison, the metrics for the representative experimental data shown in Fig. 8(a) and (b) and the baseline simulated analysis are given in Table 1.

4. Conclusions

It was shown that in the case of SEB of power devices, simulations cannot neglect the immense temperature rise resulting from power dissipation from an ion strike event. From an analytic conduction solution using voltage–current measurements as an estimate of the Joule heating in a device, the temperature resulting from a heavy ion strike was characterized for the first time. The coupled electrical and thermal solution demonstrated qualitative agreement with experimental data.

The physical model also offers the possibility of predicting thermally-induced catastrophic failure. Damage to a device is known to occur at elevated temperatures. The model can predict what temperature a particular device might reach due to radiation effects.

Incorporating temperatures in electrical simulation has not received adequate treatment to date. This work represents an effort not only to advance the state of the art in modeling temperature effects in electrical simulation, but also to demonstrate the significance of including temperature models into electrical models. Despite the low fidelity of the method used, reasonable results were obtained. However, complete modeling would necessarily include higher order effects such as thermodynamic nonequilibrium between energy carriers.

Acknowledgements

Thanks go to Scott Humphreys, Masters Student in Electrical Engineering at Vanderbilt University for his expertise in using SPICE and getting it to do things it was not designed to do. This work was supported by a Discovery Grant from Vanderbilt University.

References

[1] Waskiewicz AE, Groninger JW, Strahan VH, Long DM. Burnout of power MOS transistors with heavy ions of 252-Cf. IEEE Trans Nucl Sci 1986;33:1710.
[2] Ma PT, Dressendorfer PV. Ionizing radiation effects in MOS devices and circuits. New York: Wiley; 1989.
[3] Hohl JH, Johnson GH. Features of the triggering mechanism for single event burnout of power MOSFETs. IEEE Trans Nucl Sci 1989;36(6):2260.
[4] Hohl JH, Galloway KF. Analytical model for single event burnout of power MOSFETs. IEEE Trans Nucl Sci 1987;34(6):1275.
[5] Johnson GH, Palau J, Dachs C, Galloway KF, Schrimpf RD. A review of the techniques used for modeling single-event effects in power MOSFETs. IEEE Trans Nucl Sci 1996;43:546.
[6] Johnson GH, Hohl JH, Schrimpf RD, Galloway KF. Simulating single-event burnout of n-channel power MOSFET's. IEEE Trans Electron Dev 1993;40(5):1001.
[7] Liu J. Modeling of single event burnout in n-channel power MOSFETs. Master's Thesis, Vanderbilt University, Nashville, TN, 2000.
[8] Roubaud F, Dachs C, Palau JM, Gasiot J, Tastet P. Experimental and 2D simulation study of the single-event burnout in n-channel power MOSFET's. IEEE Trans Nucl Sci 1993;40(6):1952.
[9] Lorfevre E, Dachs C, Detcheverry C, Palau JM, Gasiot J, Roubaud F, Calvert MC, Ecoffet R. Heavy ion induced failures in a power IGBT. IEEE Trans Nucl Sci 1997; 44(6):2353.
[10] Apanovich Y, Blakey P, Cottle R, Lyumkis E, Polsky B, Shur A, Tcherniaev A. Numerical simulation of submicrometer devices including coupled nonlocal transport and nonisothermal effects. IEEE Trans Electron Dev 1995; 42(5):890.
[11] Hefner AR, Blackburn DL. Thermal component models for electro-thermal network simulation. IEEE Transactions on Components Packaging and Manufacturing Technology Part A 1994;17(3):413.
[12] Özişik MN. Boundary value problems of heat conduction. Mineola, NY: Dover; 1968.
[13] Sze SM, Physics of semiconductor devices. 2nd ed. New York: Wiley; 1981.
[14] Tien CL, Majumdar A, Gerner FM, editors. Microscale energy transport. London: Taylor and Francis; 1998.
[15] Petegen WV, Geeraerts B, Sansen W, Graindourze B. Electrothermal simulation and design of integrated circuits. IEEE J Solid State Circ 1994;29(2):143.